



**HAL**  
open science

## **Exciton Cooling in 2D Perovskite Nanoplatelets: Rationalized Carrier-Induced Stark and Phonon Bottleneck Effects**

Carolina Villamil Franco, Gaëlle Trippé-Allard, Benoît Mahler, Christian Cornaggia, Jean-sébastien Lauret, Thomas Gustavsson, Elsa Cassette

► **To cite this version:**

Carolina Villamil Franco, Gaëlle Trippé-Allard, Benoît Mahler, Christian Cornaggia, Jean-sébastien Lauret, et al.. Exciton Cooling in 2D Perovskite Nanoplatelets: Rationalized Carrier-Induced Stark and Phonon Bottleneck Effects. *Journal of Physical Chemistry Letters*, 2022, 13 (1), pp.393-399. 10.1021/acs.jpcclett.1c03894 . hal-03514245

**HAL Id: hal-03514245**

**<https://hal.science/hal-03514245>**

Submitted on 17 Feb 2022

**HAL** is a multi-disciplinary open access archive for the deposit and dissemination of scientific research documents, whether they are published or not. The documents may come from teaching and research institutions in France or abroad, or from public or private research centers.

L'archive ouverte pluridisciplinaire **HAL**, est destinée au dépôt et à la diffusion de documents scientifiques de niveau recherche, publiés ou non, émanant des établissements d'enseignement et de recherche français ou étrangers, des laboratoires publics ou privés.

# Exciton Cooling in 2D Perovskite Nanoplatelets: Rationalized Carrier-Induced Stark and Phonon Bottleneck Effects

*Carolina Villamil Franco<sup>1</sup>, Gaëlle Trippé-Allard<sup>2</sup>, Benoît Mahler<sup>3</sup>, Christian Cornaggia<sup>1</sup>, Jean-Sébastien Lauret<sup>2</sup>, Thomas Gustavsson<sup>1</sup>, and Elsa Cassette<sup>1,2,\*</sup>*

<sup>1</sup>Université Paris-Saclay, CEA, CNRS, Laboratoire Interactions, Dynamiques et Lasers (LIDYL), 91191 Gif-sur-Yvette, France. <sup>2</sup>Université Paris-Saclay, ENS Paris-Saclay, CNRS, CentraleSupélec, Laboratoire Lumière, Matière et Interfaces (LuMIn), 91405 Orsay, France. <sup>3</sup>Université de Lyon, Université Claude Bernard Lyon 1, CNRS, Institut Lumière Matière (iLM), F-69622 Villeurbanne, France.

AUTHOR INFORMATION

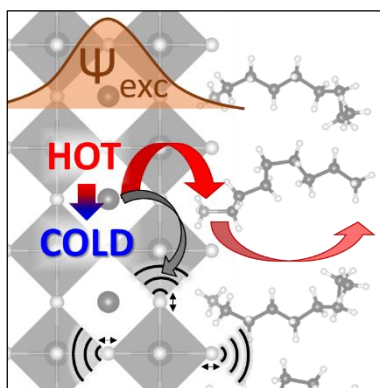
**Corresponding Author**

\*Corresponding author: [elsa.cassette@universite-paris-saclay.fr](mailto:elsa.cassette@universite-paris-saclay.fr)

## ABSTRACT

Using femtosecond transient absorption (fs-TA), we investigate the hot exciton relaxation dynamics in strongly confined lead iodide perovskite nanoplatelets (NPLs). The large quantum and dielectric confinement leads to discrete excitonic transitions and strong Stark features in the TA spectra. This prevents the use of conventional relaxation analysis methods extracting the carrier temperature or measuring the build-up of the band-edge bleaching. Instead, we show that the TA spectral lineshape near the band-edge reflects the state of the system, which can be used to probe the exciton cooling dynamics. The ultrafast hot exciton relaxation in one- to three-monolayer-thick NPLs confirms the absence of intrinsic phonon bottleneck. However, excitation fluence-dependent measurements reveal a hot phonon bottleneck effect, which is found independent on the nature of the internal cations but strongly affected by the ligands and/or sample surface state. Together, these results suggest a role of the surface ligands in the cooling process.

## TOC GRAPHIC



**KEYWORDS** hot exciton relaxation, colloidal semiconductor nanostructures, Stark effects, phonon bottleneck, femtosecond transient absorption, global analysis.

The rate at which hot charge carriers relax to the band-edge in semiconductor materials has crucial implications for the optoelectronic device performances. For instance, a slow cooling rate could allow harvesting the hot charge carriers to boost the efficiency of single junction solar cells from the theoretical Shockley-Queisser limit from 33 % to about 66%.<sup>1</sup> In contrast, fast cooling dynamics are preferred in materials for light emitting devices such as lasers and diodes. As two-dimensional (2D) halide perovskites have emerged as promising materials for such applications, it becomes crucial to scrutinize the photophysics and exciton dynamics in these samples. Several groups have investigated the hot charge-carrier/exciton relaxation (*i.e.* cooling) in halide perovskite samples: For bulk or weakly confined samples where the main excited species are free charge carriers, the cooling process is typically analyzed with femtosecond pump-probe spectroscopy.<sup>1-7</sup> Time-dependent carrier temperatures are extracted by fitting the high-energy tail of the band-edge bleaching in the transient spectra, which reflects the population of the continuous energy levels above the bandgap.<sup>1,8</sup> Cooling dynamics in halide perovskites typically range within several hundreds of femtoseconds for low excitation fluences but are strongly delayed to several orders of magnitude at high charge carrier density (starting at about  $10^{18} \text{ cm}^{-3}$ ).<sup>2-4,9</sup> This hot phonon bottleneck effect, commonly observed in inorganic polar semiconductors, is linked to the reabsorption of long-lived longitudinal optical (LO) phonons, while their interaction with the hot charge carriers controls the first step of the relaxation.<sup>4,10</sup> In strongly confined nanostructures, another strong reduction of the cooling rate is expected already at low exciton density, when the energy level separations become larger than the energy of relevant optical phonon modes.<sup>11</sup> However, this intrinsic phonon bottleneck is hardly observed in colloidal semiconductor nanostructures due to other fast relaxation pathways.<sup>12-15</sup> In halide perovskite nanocrystals (NCs), a slightly slower cooling rate was observed within smaller sized MAPbBr<sub>3</sub> nanocubes,<sup>16</sup> whereas

in more recent studies, similar relaxation dynamics were reported for CsPbBr<sub>3</sub> and FAPbBr<sub>3</sub> NCs over a larger size range.<sup>17,18</sup> Furthermore, ultrafast cooling times were reported in few monolayer-thick two-dimensional (2D) perovskites, such as one monolayer ( $n=1$ ) lead iodide-based films<sup>19,20</sup> and three monolayer ( $n=3$ ) colloidal NPLs.<sup>21</sup> Curiously, the absence of a hot phonon bottleneck effect at high excitation fluence was argued in this last study.

Here, we examined the hot exciton relaxation dynamics of hybrid (formamidinium, FA- or methylammonium, MA- based) and inorganic (Cs-based and single monolayer) lead iodide perovskite NPLs excited well-above the optical bandgap, using femtosecond TA spectroscopy. With a global analysis method, we show that the cooling dynamics can be well-described in the perovskite NPL system by an evolution from a “hot” excited state to a “relaxed” one, with characteristic TA features and rates. We found faster intrinsic cooling times in the thinner NPLs, which are however delayed at high excitation fluence for all samples. This hot phonon bottleneck effect is enhanced when comparing the colloidal NPL results with those of 2D perovskite films.

We started by investigating the hot exciton relaxation dynamics in two-monolayer thick colloidal NPLs with FA<sup>+</sup> as internal cations between the lead iodide sheets (FAPI  $n=2$ , see characterizations in supporting information, SI, **Figures S1** and **S2c**). We used fs-TA with a pump at 400 nm (3.1 eV), leading to an excess energy of about 950 meV above the optical bandgap. The temporal resolution is about 100 fs (**Figure S3**, see description of the TA setup in the SI). The early time-dependent transient spectra  $\Delta A(\lambda)$  for a low excitation fluence are displayed in **Figure 1a**. The spectra are dominated by a strong and narrow negative feature around 576 nm, matching the energy of the first excitonic transition in the linear absorption (**Figure S1a**). Moreover, two strong positive signals surround this negative signal, rising directly within the pump-probe time overlap ( $T=0-100$  fs) and persist well after the pump duration. This leads to an overall lineshape of a second

derivative of a Lorentzian function. At longer times ( $> 300$  fs), the low-energy positive signal become weaker. Then, the spectra do not change in shape after a few picoseconds (**Figure S5** in SI) and are further independent on the initial excitation energy (**Figure S6**). Thus, the later time negative signal at 576 nm should reflect, at least in part, the photo-induced bleaching (PIB) of the first excitonic transition due to state filling of the band-edge states. We will show in the following that the extra signals are consistent with carrier-induced Stark effects that, with the PIB, reflect the state of the system (*e.g.* a “hot” or a “relaxed” state). Thus, the evolution in time of the TA spectra can be used to extract the cooling dynamics, as previously reported in other semiconductor nanocrystals.<sup>22–24</sup> Importantly, here the first excitonic transition is discrete and no high-energy tail in the PIB can be observed (nor fitted) due to the absence of continuous energy levels right above the optical bandgap. This, together with the modulation of the spectral lineshape due to the different photo-physical phenomena, prevents the use of classical analysis of the cooling process.

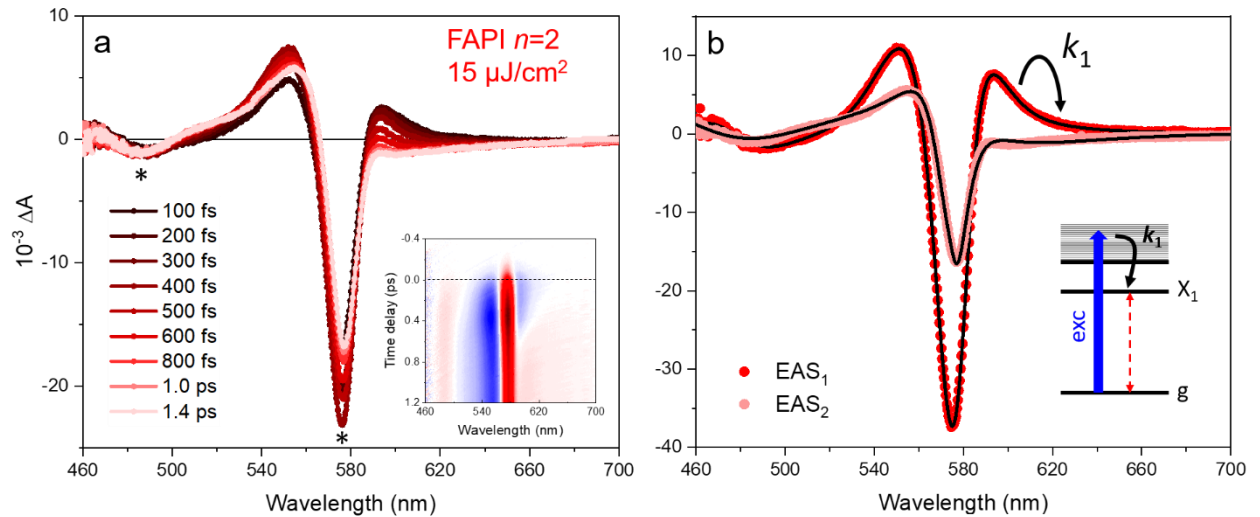


**Figure 1.** (a) Low fluence, time-dependent TA spectra of FAPI  $n=2$  NPLs during the stage of hot exciton relaxation (pump at 400 nm). The first and second excitonic transitions are marked with an asterisk (\*). Inset: full TA map. (b) Corresponding evolution associated spectra (EAS, red and

pink dots) obtained with global analysis using a sequential kinetic model with two components. The rate  $k_1$  characterizes the cooling process. The EAS were fitted (in black) by modeling the change of the absorption in terms of amplitude, center energy and linewidth (see SI). Inset: schematics of the cooling process to the band-edge after high-energy excitation in the continuum of states.

We thus used a global target analysis<sup>25</sup> with a sequential model<sup>8</sup> to fit the full evolution of the TA spectra in time and extract the initial and final state associated spectra (EAS<sub>1</sub>), as well with the characteristic rates ( $k_i$ ) of their temporal evolution. For FAPI  $n=2$  NPLs at low excitation fluence, the full TA data are well-modeled by two spectral and kinetic components, displayed in **Figure 1b**: EAS<sub>1</sub> appearing within the pump pulse and decaying exponentially with a characteristic time  $\tau_1=1/k_1$  (here about 270 fs) and EAS<sub>2</sub> growing exponentially with  $\tau_1$  and decaying in amplitude with  $\tau_2=1/k_2$ , of a few orders of magnitude larger than  $\tau_1$ . The good agreement between the experimental data and the global fit is illustrated in the dynamics **Figure S7** of the SI. Here the  $\tau_1$ , extracted from global analysis and which characterizes the evolution from EAS<sub>1</sub> to EAS<sub>2</sub>, is the characteristic time of the exciton cooling, as we will explain below by rationalizing the EAS lineshape in terms of carrier-induced Stark signals and PIB.

The second derivative lineshape of the initial EAS<sub>1</sub> spectrum for a low excitation fluence is characteristic of a *broadening* of the first absorption peak with the pump “on”. It can be attributed to a *pure Stark effect* involving shifts towards both low- and high-energies (**Figure S8a,b**), without significant “bleaching” component (almost no change of amplitude). This was confirmed by the simulations of the transient spectra displayed **Figure 1b** (and **Figure S9a**, see SI for details), where we modeled the change of absorption of the band-edge transition in terms of amplitude, linewidth and center energy (see SI):<sup>19</sup> The relative change in linewidth of the band-edge absorption, ( $\omega_{\text{ON-}}$

$\omega_{\text{OFF}})/\omega_{\text{OFF}} = \Delta\omega/\omega_0$ , is about 33 % for the smallest excitation fluence, while the relative change in area,  $(A_{\text{ON}}-A_{\text{OFF}})/A_{\text{OFF}} = \Delta A/A_0$ , is only about -0.3 %. The pure derivative-like lineshape of EAS<sub>1</sub> at low fluence evidences that, for 400 nm excitation, initially both excited electron and hole populate states higher in energy than the excited state corresponding to the band-edge transition. Here the Stark signal results from the high-energy electron-hole pair created by the pump pulse, which induces an internal electric field that shifts the energy of all probed optical transitions. For the well-defined band-edge excitonic transition with associated dipole expected in the plane of the NPL,<sup>26</sup> different derivative lineshapes can be obtained (**Figure S8**): On the one hand, an electric field in the NPL plane (thus parallel to the probed transition dipole) induces some spatial separation of the electron and hole wavefunction, leading to a decrease of the exciton binding energy, which results in a high-energy shift of the optical transition. On the other hand, an electric field perpendicular to the NPL plane should result in a red shift,<sup>27,28</sup> known as a quantum-confined Stark effect, with little variation on the exciton binding energy at low/moderate field value.<sup>27</sup> These blue- (red-) shifts are characteristic of the effect of an electric field applied in (perpendicular to) the 2D plane of quantum wells, as typically observed in epitaxially grown nanostructures.<sup>29,30</sup> These two contributions are observed at the same time, as for a pump excitation well above the band-edge, there should not be any photo-selection of a special dipole orientation. In other words, the excitation well above the bandgap generates dipoles with statistically random orientations. Indeed, at this energy away from the confinement effects, multiple resonant transitions with a dipole in and out of the 2D plane are expected to be excited within the polarized excitation.<sup>31,32</sup> Thus, the random electric field leads to both high- and low- energy shifts resulting in a *broadening* of the probed band-edge optical transition, which gives an overall second derivative lineshape in the TA spectra (**Figure S8c**).

In contrast, the EAS<sub>2</sub> at low excitation fluence displays mostly an asymmetric first derivative lineshape, with main characteristics of a *unidirectional shift*, towards high energies (**Figure 1b**). Compared to a pure derivative lineshape, the negative contribution is much more pronounced than the positive one. Part of this negative signal can be associated to the reduction of absorption due to the state filling effect (*i.e.* population of the band-edge states), while the derivative lineshape (positive and negative signals) still results from Stark effects, induced now by the relaxed exciton initially created by the pump. In fact, the blue-shift can be seen as the effect of an internal electric field applied parallel to the dipole of the probed transition (*i.e.* in the NPL 2D plane), as mentioned above. The EAS<sub>2</sub> spectrum is thus characteristic of the relaxed (cooled-down) excited state.

We then investigated the effect of high excitation fluence on relaxation dynamics of these FAPI  $n=2$  NPLs. Similar but broader TA features were observed for these higher excitation fluences (**Figure S10a** in the SI). Again, no high-energy tail can be fitted in the band-edge PIB for these 2D structures, in contrast with the work of Ding *and co.*<sup>33</sup> The TA features are rather symmetrically broadened, similarly to what was previously observed in TA in CdSe NPLs.<sup>34</sup> Global analysis required a slightly more complex sequence, with initial spectral (EAS<sub>0</sub>) and rate ( $k_0$ ) components and eventually a coherent artifact, in order to fit these TA data more properly (see SI, EAS<sub>2</sub> and fit **Figures S10b**, decays **Figure S7**, fit quality **Figure S11b**). Here, the evolution from EAS<sub>1</sub> to EAS<sub>2</sub> still describes the hot exciton cooling dynamics. The change of band-edge transition linewidth as a function of excitation fluence is more pronounced in EAS<sub>1</sub> than in EAS<sub>2</sub>, with no or much reduced PIB contribution (**Figure S9c,d**). We note however that at excitation fluence above 80  $\mu\text{J}/\text{cm}^2$ , the relative change in the absorption area becomes non-negligible and increases with the excitation fluence. This is explained by a change of oscillator strength due to exciton-exciton interactions rather by a state filling effect, as seen previously.<sup>19</sup> Indeed, the

threshold of  $80 \mu\text{J}/\text{cm}^2$  observed for FAPI  $n=2$  NPLs corresponds to an exciton density of about  $5 \times 10^{12} \text{ cm}^{-2}$ . We have shown previously that such high density involves that the numerous excitons photogenerated in the NPLs spatially overlap, such as the resulting Auger recombination is not diffusion-limited anymore.<sup>35</sup> Importantly, we clearly observe slower cooling dynamics with increasing excitation fluence (**Figure S11a**). The hot exciton cooling time is delayed to almost 1 ps for the highest excitation fluence, while the fluence-dependence is noticed starting at the  $80 \mu\text{J}/\text{cm}^2$  fluence threshold for this NPL sample. This delayed relaxation could however uneasily be explained by Auger reheating effects as exciton-exciton Auger recombination occurs with a longer characteristic time of several picoseconds in these NPL systems at that high exciton density.<sup>35</sup> This effect was thus attributed to the hot phonon bottleneck, as measured in weakly confined nanostructures of FAPbI<sub>3</sub>.<sup>8,36</sup> However, the intrinsic cooling time (*i.e.* at low excitation fluence) was found much faster, leading to an energy-loss rate of about  $3.5 \text{ eV} \cdot \text{ps}^{-1}$ .

In few monolayer thick 2D perovskite films and colloidal NPLs with a first exciton binding energy of a few hundreds of meV, the continuum of states is well above the discrete first excitonic transition.<sup>37</sup> Thus, no high-energy tail in the lowest energy PIB can be exploited to characterize the distribution of population in the early time of the TA spectra, due to the absence of underlying continuum of states. Feldmann *and co.*<sup>21</sup> have proposed to extract the relaxation dynamics of  $n=3$  MA-based perovskite NPLs by fitting the high-energy tail of a higher energy peak, corresponding to the second excitonic transition, which overlaps with the continuum of states in energy. From our point of view, such approach probes the relaxation from higher, continuum-like, levels. Here instead, we investigated the effect of the confinement by focusing on the last stage of relaxation to the discrete lowest energy states. Furthermore, the method of Feldmann *and co.* cannot be applied in thinner NPL samples such as  $n=2$  and  $n=1$  where the second excitonic transition is still below

the continuum of states. Finally, at high excitation fluence, the depopulation of higher-energy excitonic states will be ensured by the Auger recombination process rather than cooling, which will thus not help us to clarify the mechanism of relaxation. Another reported approach to investigate the cooling dynamics consists in following the band-edge state population from the PIB growth of the corresponding first excitonic transition.<sup>38</sup> However, here the PIB has to be disentangled from the instantaneously-rising Stark signals, from the interaction between the pump exciton/charge-carriers and the probe exciton. Here indeed, we observe an effective *decrease* of the band-edge “bleaching” amplitude in time instead of a *build-up* (**Figure 1** and **S7**).

To get more insight on the cooling process, we performed the same kind of experiments with 400 nm excitation and applied similar analysis, on lead iodide perovskite NPL samples of different number of monolayers and different compositions. The steady-state absorption spectra and photoluminescence of the different samples are displayed in **Figure S1**. The experimental TA spectra of  $n=1$  (with butyl-ammonium ligands, Bu-PI), CsPI and MAPI  $n=2$  and MAPI  $n=3$  NPLs are displayed in **Figure 2 (Figure S12)** for low (high) excitation fluences. Corresponding global analysis results are shown in **Figure S13** in the SI. We first compared the results obtained at low excitation fluence. The EAS spectral lineshapes were found similar than those of the corresponding EASs of FAPI  $n=2$  NPL samples, which then allows us to compare the associated intrinsic cooling time  $\tau_1 = 1/k_1$ . For the thinner NPL samples (*i.e.*  $n=1$ ), we found the faster relaxation kinetics at low excitation fluence, with  $\tau_1 = 190\text{-}250$  fs. For  $n=2$  NPLs, we found very similar intrinsic cooling times for MAPI and FAPI, with  $\tau_1 = 270\text{-}280$  fs. Importantly, we obtained a significantly longer cooling time of about 360-370 fs for the thicker NPL sample, MAPI  $n=3$ . This is longer than the value reported by Feldmann *and co.* considering the relaxation within the continuum of states.<sup>21</sup> We found by performing excitation energy-dependent experiments, that the

cooling rate is limited by the last relaxation step to the discrete band-edge states (**Figure S15**). Thus, the difference of excess energy used in the experiments cannot by itself explain the difference of relaxation times between the NPL samples of different thicknesses. In addition, within the same thickness, the cooling time was longer for the Cs-based NPL samples CsPI  $n=2$ , with  $\tau_1 = 350\text{-}370$  fs. This is in agreement with the slower relaxation expected for these perovskite samples with inorganic  $\text{Cs}^+$  cations compared to the hybrid counterparts, as they possess less internal vibrational modes.<sup>18,39</sup>

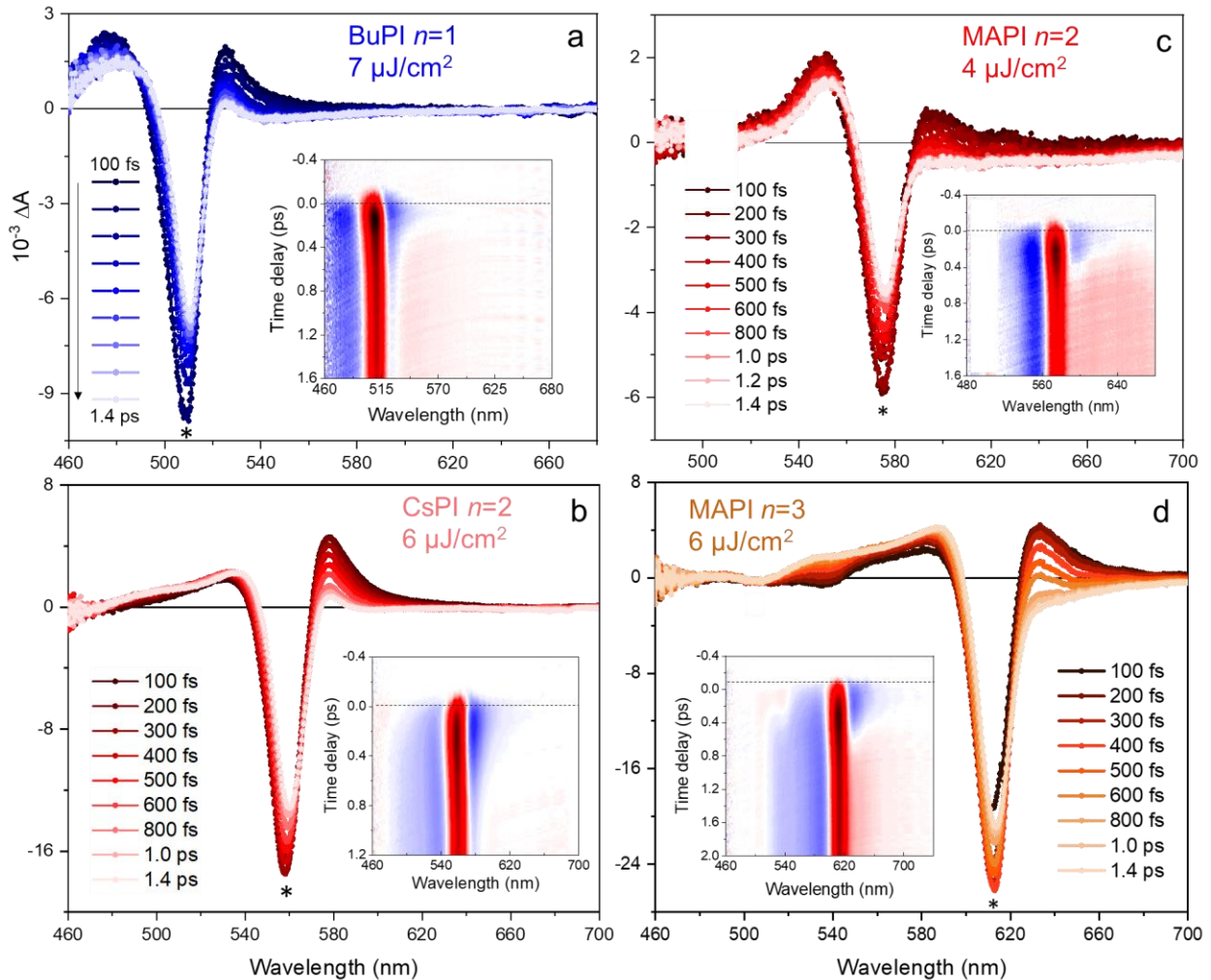


**Figure 2:** TA spectra of Bu-PI  $n=1$  (a), MAPI and CsPI  $n=2$  (b and c, respectively) and MAPI  $n=3$  NPLs for a low excitation fluence at 400 nm. First excitonic transitions are marked with a star. The full TA map are displayed in inset with the negative signals in red, the positive in blue, and  $\Delta A=0$  in white.

The absence of an intrinsic phonon bottleneck and the unexpected faster dynamics in the thinner NPL samples suggest the presence of an additional relaxation pathway, which seems more efficient with increasing confinement. This is in agreement with the results of Wu and co-workers in confined CsPbBr<sub>3</sub> nanocrystals.<sup>17</sup> Now looking at the fluence-dependent experiments, we found for all the NPL samples that the extracted cooling times increase with increasing excitation fluence, up to about almost 1 ps (**Figure 3, S11a and S16**), consistently with the hot phonon bottleneck effect. The similar linear absorption coefficient of MA-, FA- and Cs- lead iodide perovskites should allow a direct comparison between NPLs of the same thickness, as in that case the initial exciton density (*i.e.* number of excitons per cm<sup>2</sup>) is proportional to the excitation fluence at high energy with a very similar scaling factor (see SI for details). In addition, we more specifically compared the NPL samples measured within the same couples of days, with similar experimental conditions (*i.e.* same pump compression and waist dimension). In bulk lead iodide perovskite film, the hot phonon bottleneck effect was found to be more pronounced for fully inorganic Cs-based perovskites than in the hybrid ones.<sup>5</sup> This was again explained by the role of additional molecular vibrational modes and/or dynamic disorder in the latter due to the organic cation rotation.<sup>5,18,39</sup> Here however, when comparing the dependency of the exciton cooling time on the excitation fluence (the slope) for  $n=2$  NPLs with different cations (**Figure 3a**), we found no clear difference between CsPI and the hybrid-based samples. This similarity between fully-inorganic and the hybrid perovskite NPLs is an additional clue in support of the hypothesis that the exciton cooling

process in these 2D nanostructures is dominated by a different mechanism than the classical energy dissipation *via* the coupling to vibrational modes *within* the crystalline structure. However, a “hot phonon bottleneck” effect is indeed observed but independent on the nature of the A<sup>+</sup> cations. This needs to be rationalized by another mechanism than the reabsorption of long-lived LO phonons at high exciton density.

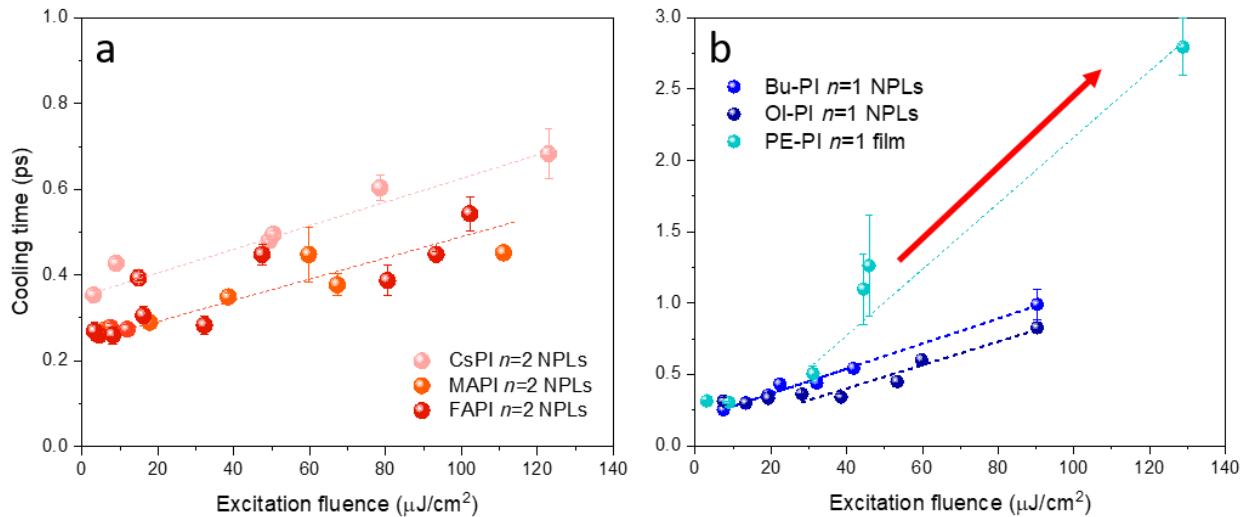


**Figure 3.** Evolution of the cooling times obtained with global analysis with the excitation fluence, in  $n=2$  NPLs to investigate the effect of the cations (a) and in  $n=1$  NPLs and 2D film to investigate the effect of the ligands (b). Dashed lines are visual aid of the cooling time to excitation fluence dependency. The enhanced “hot phonon bottleneck” effect in the film is highlighted by the red arrow.

In small nanocrystals and 2D perovskites, the absence of an intrinsic phonon bottleneck in the cooling dynamics was suggested to result from non-adiabatic relaxation pathways involving multiphonon emission and/or coupling to surface ligand vibrational modes,<sup>17,19,21</sup> in analogy with reports on II-VI and III-V semiconductor quantum dots.<sup>14,40</sup> Here, the very similar slope of the fluence-dependent hot exciton cooling times between the inorganic (CsPI) and hybrid (FAPI and

MAPI) NPL samples **Figure 3a** is rather inconsistent with a multiphonon emission process. Indeed, in that case the cooling rate would be highly dependent on the Huang-Rhys factor  $S$  (power dependence with the number of involved phonons), itself largely dependent on the density of available vibrational modes.<sup>41</sup> Alternatively, the role played by the surface ligands in the cooling mechanism might explain why faster cooling times are measured within the more strongly-confined systems: the decrease of thickness enhances the coupling between the ligand vibrational modes and the exciton which wavefunction is more delocalized outside the lattice framework. Previous studies based on perovskite nanocrystals have investigated the role of surface ligands in the cooling dynamics and have concluded the absence of such effect.<sup>17,18,42</sup> However, the typical size of the nanocrystals was ranging from about 3 to 13 nm. In contrast, our NPLs have a thickness of 1 to 3 monolayers (about 0.6 to 1.8 nm) and result in substantial faster cooling times. This motivated us to performed experiments by varying the nature of the surface ligands. We use  $n=1$  2D perovskites as model samples to study the effect of the *external* ammonium cations on the hot exciton relaxation. However, as the ammonium ligands are part of the 2D perovskite crystalline structure, they cannot be exchanged as simply as for nanocrystals. We thus studied colloidal NPLs with short (butyl-) and long (oleyl-) ammonium ligands and compared them with 2D Ruddlesden-Popper thin film with identical number of MLs ( $n=1$ ). The corresponding linear absorption spectra are shown in **Figure S17**. The cooling times are displayed in **Figure 3b** for the different excitation fluences. Results on 2D perovskite films show significantly larger dependency on the excitation fluence, as seen with an enhanced hot phonon bottleneck effect. Per opposition with the internal organic cations, ligands in the colloidal NPL systems are in direct contact with the surrounding medium (solvent) and can then easily release the excess energy, limiting thus the “hot phonon bottleneck” effect at high excitation fluence. In contrast, the ligands in 2D layered perovskite thin

film are expected to be “frozen” in between layers. This might result in a back energy transfer, in analogy with the optical phonon reabsorption or acoustic phonon upconversion processes taking place within the crystalline structure involving/leading to LO phonons with long lifetime.<sup>1</sup> We note that such a large difference in the measured slope **Figure 3b** between the 2D film and colloidal NPL samples cannot be explained by a simple effect of exciton mobility in the magnitude of exciton-exciton interactions induced by a difference of ligands (phenylethyl- versus linear alkyl-ammoniums).<sup>43</sup> Indeed, here the hot phonon bottleneck effect is observed in the regime of overlapping excitons, as discussed above. Furthermore, one can notice the absence of a clear difference in the intrinsic relaxation time between the  $n=1$  perovskite samples (colloidal NPLs and 2D films). This seems to imply that the difference of slope cannot just result from the difference of quantum well rigidity (*i.e.* modification of the coupling strength with the phonons). In addition, the similarity of the intrinsic cooling times suggests that the difference of the ligand dielectric constant on the cooling dynamics, although investigated theoretically and experimentally in 2D RP films,<sup>44</sup> does not seem to be a key parameter.

In conclusion, we have investigated the ultrafast dynamics of strongly confined 2D lead iodide perovskite NPLs of one to three monolayers, using femtosecond transient absorption with excitation well above the band-edge. The exciton cooling rate was determined with a global analysis method and the associated spectral components were rationalized in terms of large carrier-induced Stark and bleaching signals. The faster cooling rate in the thinner NPL samples confirmed the absence of an intrinsic phonon bottleneck. Interestingly, replacing the molecular cations ( $\text{FA}^+$  or  $\text{MA}^+$ ) with inorganic ones ( $\text{Cs}^+$ ) does not affect the evolution of the cooling rate with the excitation fluence. However, our results support the role of molecular vibrations of the external ammonium ligands at the surface of the NPLs and their coupling to the environment bath to

dissipate the excess energy within the hot exciton relaxation process. An enhanced hot phonon bottleneck effect is indeed observed at high excitation fluences in 2D perovskite films when comparing the cooling rates to those of the colloidal NPLs. Then, surface design and engineering should allow a control of the cooling rate in these 2D perovskite nanostructures in order to obtain highly performant optoelectronic devices.

## ASSOCIATED CONTENT

### **Supporting Information.**

The following files are available free of charge: Description of the NPL sample preparation and characterizations; description of the fs-TA setup and data analysis; additional TA data; details of the spectrum simulation; additional global analysis data; calculation of the exciton density and extra linear absorption spectra.

## AUTHOR INFORMATION

### **Notes**

The authors declare no competing financial interests.

## ACKNOWLEDGMENTS

This work was supported by the French Agence Nationale de la Recherche (grant ANR-16-ACHN-0022-01). C.V.F thanks the University Paris-Saclay for the Ecole Doctorale 2MIB Scholarship. C.C. thanks the LabEx PALM of Paris-Saclay University (ANR-10-LABX-0039-PALM), overseen by the ANR under the framework “Investissements d’avenir”.

## REFERENCES

- (1) Li, M.; Fu, J.; Xu, Q.; Sum, T. C. Slow Hot-Carrier Cooling in Halide Perovskites: Prospects

- for Hot-Carrier Solar Cells. *Adv. Mater.* **2019**, *31* (47), 1802486.
- (2) Price, M. B.; Butkus, J.; Jellicoe, T. C.; Sadhanala, A.; Briane, A.; Halpert, J. E.; Broch, K.; Hodgkiss, J. M.; Friend, R. H.; Deschler, F. Hot-Carrier Cooling and Photoinduced Refractive Index Changes in Organic–Inorganic Lead Halide Perovskites. *Nat. Commun.* **2015**, *6* (1), 8420.
  - (3) Yang, Y.; Ostrowski, D. P.; France, R. M.; Zhu, K.; Van De Lagemaat, J.; Luther, J. M.; Beard, M. C. Observation of a Hot-Phonon Bottleneck in Lead-Iodide Perovskites. *Nat. Photonics* **2016**, *10* (1), 53–59.
  - (4) Fu, J.; Xu, Q.; Han, G.; Wu, B.; Huan, C. H. A.; Leek, M. L.; Sum, T. C. Hot Carrier Cooling Mechanisms in Halide Perovskites. *Nat. Commun.* **2017**, *8* (1).
  - (5) Hopper, T. R.; Gorodetsky, A.; Frost, J. M.; Müller, C.; Lovrincic, R.; Bakulin, A. A. Ultrafast Intraband Spectroscopy of Hot-Carrier Cooling in Lead-Halide Perovskites. *ACS Energy Lett.* **2018**, *3* (9), 2199–2205.
  - (6) Zhu, H.; Miyata, K.; Fu, Y.; Wang, J.; Joshi, P. P.; Niesner, D.; Williams, K. W.; Jin, S.; Zhu, X. Screening in Crystalline Liquids Protects Energetic Carriers in Hybrid Perovskites. *Science* (80-. ). **2016**, *353* (6306), 1409–1413.
  - (7) Trinh, M. T.; Wu, X.; Niesner, D.; Zhu, X. Many-Body Interactions in Photo-Excited Lead Iodide Perovskite. *J. Mater. Chem. A* **2015**, *3* (17), 9285–9290.
  - (8) Franco, C. V.; Mahler, B.; Cornaggia, C.; Gustavsson, T.; Cassette, E. Charge Carrier Relaxation in Colloidal FAPbI<sub>3</sub> Nanostructures Using Global Analysis. *Nanomaterials* **2020**, *10* (10), 1897.
  - (9) Yang, J.; Wen, X.; Xia, H.; Sheng, R.; Ma, Q.; Kim, J.; Tapping, P.; Harada, T.; Kee, T. W.; Huang, F.; Cheng, Y-B.; Green, M.; Ho-Baillie, A.; Huang, S.; Shrestha, S.; Patterson,

- R.; Conibeer, G. Acoustic-Optical Phonon up-Conversion and Hot-Phonon Bottleneck in Lead-Halide Perovskites. *Nat. Commun.* **2017**, *8* (1), 14120.
- (10) Ridley, B. K. *Quantum Processes in Semiconductors*, Oxford.; Oxford University Press, 2013.
- (11) Nozik, A. J. Spectroscopy and Hot Electron Relaxation Dynamics in Semiconductor Quantum Wells and Quantum Dots. *Annu. Rev. Phys. Chem.* **2001**, *52*, 193–231.
- (12) Efros, A. L.; Kharchenko, V. A.; Rosen, M. Breaking the Phonon Bottleneck in Nanometer Quantum Dots: Role of Auger-like Processes. *Solid State Commun.* **1995**, *93* (4), 281–284.
- (13) Klimov, V. I.; Mikhailovsky, a.; McBranch, D.; Leatherdale, C. A.; Bawendi, M. G. Mechanisms for Intraband Energy Relaxation in Semiconductor Quantum Dots: The Role of Electron-Hole Interactions. *Phys. Rev. B* **2000**, *61* (20), R13349–R13352.
- (14) Cooney, R.; Sewall, S.; Anderson, K. E. H.; Dias, E. A.; Kambhampati, P. Breaking the Phonon Bottleneck for Holes in Semiconductor Quantum Dots. *Phys. Rev. Lett.* **2007**, *98* (17), 177403.
- (15) Peterson, M. D.; Cass, L. C.; Harris, R. D.; Edme, K.; Sung, K.; Weiss, E. A. The Role of Ligands in Determining the Exciton Relaxation Dynamics in Semiconductor Quantum Dots. *Annu. Rev. Phys. Chem.* **2014**, *65* (1), 317–339.
- (16) Li, M.; Bhaumik, S.; Goh, T. W.; Kumar, M. S.; Yantara, N.; Grätzel, M.; Mhaisalkar, S.; Mathews, N.; Sum, T. C. Slow Cooling and Highly Efficient Extraction of Hot Carriers in Colloidal Perovskite Nanocrystals. *Nat. Commun.* **2017**, *8* (1), 14350.
- (17) Li, Y.; Lai, R.; Luo, X.; Liu, X.; Ding, T.; Lu, X.; Wu, K. On the Absence of a Phonon Bottleneck in Strongly Confined CsPbBr<sub>3</sub> Perovskite Nanocrystals. *Chem. Sci.* **2019**, *10* (23), 5983–5989.

- (18) Diroll, B. T.; Schaller, R. D. Intraband Cooling in All-Inorganic and Hybrid Organic–Inorganic Perovskite Nanocrystals. *Adv. Funct. Mater.* **2019**, *29* (37), 1901725.
- (19) Abdel-Baki, K.; Boitier, F.; Diab, H.; Lanty, G.; Jemli, K.; Lédée, F.; Garrot, D.; Deleporte, E.; Lauret, J. S. Exciton Dynamics and Non-Linearities in Two-Dimensional Hybrid Organic Perovskites. *J. Appl. Phys.* **2016**, *119* (6), 064301.
- (20) Wu, X.; Trinh, M. T.; Zhu, X. Excitonic Many-Body Interactions in Two-Dimensional Lead Iodide Perovskite Quantum Wells. *J. Phys. Chem. C* **2015**, *119* (26), 14714–14721.
- (21) Hintermayr, V. A.; Polavarapu, L.; Urban, A. S.; Feldmann, J. Accelerated Carrier Relaxation through Reduced Coulomb Screening in Two-Dimensional Halide Perovskite Nanoplatelets. *ACS Nano* **2018**, *12* (10), 10151–10158.
- (22) Kambhampati, P. Unraveling the Structure and Dynamics of Excitons in Semiconductor Quantum Dots. *Acc. Chem. Res.* **2011**, *44* (1), 1–13.
- (23) Klimov, V. I.; McBranch, D. Femtosecond 1P-to- 1S Electron Relaxation in Strongly Confined Semiconductor Nanocrystals. *Phys. Rev. Lett.* **1998**, *80* (18), 4028–4031.
- (24) Trinh, M. T.; Sfeir, M. Y.; Choi, J. J.; Owen, J. S.; Zhu, X. A Hot Electron-Hole Pair Breaks the Symmetry of a Semiconductor Quantum Dot. *Nano Lett.* **2013**, *13* (12), 6091–6097.
- (25) Snellenburg, J. J.; Laptinok, S. P.; Seger, R.; Mullen, K. M.; van Stockkum, I. H. M.; Stokkun, I. H. M. Glotaran: A Java-Based Graphical User Interface for the R Package TIMP. *J. Stat. Softw.* **2012**, *49* (3), 1–22.
- (26) Proppe, A. H.; Walters, G. W.; Alsalloum, A. Y.; Zhumekenov, A. A.; Mosconi, E.; Kelley, S. O.; De Angelis, F.; Adamska, L.; Umari, P.; Bakr, O. M.; Sargent, E. H. Transition Dipole Moments of  $n = 1, 2$ , and  $3$  Perovskite Quantum Wells from the Optical Stark Effect and Many-Body Perturbation Theory. *J. Phys. Chem. Lett.* **2020**, *11* (3), 716–723.

- (27) Bastard, G. *Wave Mechanics Applied to Semiconductor Heterostructures*; Physique, L. éditions de, Ed.; 1991.
- (28) Walters, G.; Wei, M.; Voznyy, O.; Quintero-Bermudez, R.; Kiani, A.; Smilgies, D. M.; Munir, R.; Amassian, A.; Hoogland, S.; Sargent, E. H. The Quantum-Confined Stark Effect in Layered Hybrid Perovskites Mediated by Orientational Polarizability of Confined Dipoles. *Nat. Commun.* **2018**, *9* (1).
- (29) Chemla, D. S. Two-Dimensional Semiconductors: Recent Development. *J. Lumin.* **1985**, *30* (1–4), 502–519.
- (30) Schmitt-Rink, S.; Chemla, D. S.; Miller, D. A. B. Linear and Nonlinear Optical Properties of Semiconductor Quantum Wells. *Adv. Phys.* 1989, pp 89–188.
- (31) Scott, R.; Heckmann, J.; Prudnikau, A. V.; Antanovich, A.; Mikhailov, A.; Owschimikow, N.; Artemyev, M.; Climente, J. I.; Woggon, U.; Grosse, N. B.; Achtstein, A. W. Directed Emission of CdSe Nanoplatelets Originating from Strongly Anisotropic 2D Electronic Structure. *Nat. Nanotechnol.* **2017**, *12* (12), 1155–1160.
- (32) Cassette, E.; Mahler, B.; Guigner, J.-M.; Patriarche, G.; Dubertret, B.; Pons, T. Colloidal CdSe/CdS Dot-in-Plate Nanocrystals with 2D-Polarized Emission. *ACS Nano* **2012**, *6* (8), 6741–6750.
- (33) Jia, X.; Jiang, J.; Zhang, Y.; Qiu, J.; Wang, S.; Chen, Z.; Yuan, N.; Ding, J. Observation of Enhanced Hot Phonon Bottleneck Effect in 2D Perovskites. *Appl. Phys. Lett.* **2018**, *112* (14), 143903.
- (34) Pelton, M.; Ithurria, S.; Schaller, R. D.; Dolzhenkov, D. S.; Talapin, D. V. Carrier Cooling in Colloidal Quantum Wells. *Nano Lett.* **2012**, *12* (12), 6158–6163.
- (35) Villamil Franco, C.; Mahler, B.; Cornaggia, C.; Gustavsson, T.; Cassette, E. Auger

- Recombination and Multiple Exciton Generation in Colloidal Two-Dimensional Perovskite Nanoplatelets: Implications for Light-Emitting Devices. *ACS Appl. Nano Mater.* **2021**, *4* (1), 558–567.
- (36) Papagiorgis, P.; Protesescu, L.; Kovalenko, M. V.; Othonos, A.; Itskos, G. Long-Lived Hot Carriers in Formamidinium Lead Iodide Nanocrystals. *J. Phys. Chem. C* **2017**, *121* (22), 12434–12440.
- (37) Blancon, J.-C.; Stier, A. V.; Tsai, H.; Nie, W.; Stoumpos, C. C.; Traoré, B.; Pedesseau, L.; Kepenekian, M.; Katsutani, F.; Noe, G. T.; Kono, J.; Tretiak, S.; Crooker, S. A.; Katan, C.; Kanatzidis, M. G.; Crochet, J. J.; Even, J.; Mohite, A. D. Scaling Law for Excitons in 2D Perovskite Quantum Wells. *Nat. Commun.* **2018**, *9* (1), 2254.
- (38) Chung, H.; Jung, S. Il; Kim, H. J.; Cha, W.; Sim, E.; Kim, D.; Koh, W.-K.; Kim, J. Composition-Dependent Hot Carrier Relaxation Dynamics in Cesium Lead Halide (CsPbX<sub>3</sub>, X=Br and I) Perovskite Nanocrystals. *Angew. Chemie Int. Ed.* **2017**, *56* (15), 4160–4164.
- (39) Chen, J.; Messing, M. E.; Zheng, K.; Pullerits, T. Cation-Dependent Hot Carrier Cooling in Halide Perovskite Nanocrystals. *J. Am. Chem. Soc.* **2019**, *141* (8), 3532–3540.
- (40) Schaller, R. D.; Pietryga, J. M.; Goupalov, S. V.; Petruska, M. A.; Ivanov, S. A.; Klimov, V. I. Breaking the Phonon Bottleneck in Semiconductor Nanocrystals via Multiphonon Emission Induced by Intrinsic Nonadiabatic Interactions. *Phys. Rev. Lett.* **2005**, *95* (19), 1–4.
- (41) Bozyigit, D.; Yazdani, N.; Yarema, M.; Yarema, O.; Lin, W. M. M.; Volk, S.; Vuttivorakulchai, K.; Luisier, M.; Juranyi, F.; Wood, V. Soft Surfaces of Nanomaterials Enable Strong Phonon Interactions. *Nature* **2016**, *531* (7596), 618–622.
- (42) Hopper, T. R.; Gorodetsky, A.; Jeong, A.; Krieg, F.; Bodnarchuk, M. I.; Maimaris, M.;

- Chaplain, M.; Macdonald, T. J.; Huang, X.; Lovrincic, R.; Kovalenko, M. V.; Bakulin, A. A. Hot Carrier Dynamics in Perovskite Nanocrystal Solids: Role of the Cold Carriers, Nanoconfinement, and the Surface. *Nano Lett.* **2020**, *20* (4), 2271–2278.
- (43) Seitz, M.; Magdaleno, A. J.; Alcázar-Cano, N.; Meléndez, M.; Lubbers, T. J.; Walraven, S. W.; Pakdel, S.; Prada, E.; Delgado-Buscalioni, R.; Prins, F. Exciton Diffusion in Two-Dimensional Metal-Halide Perovskites. *Nat. Commun.* **2020**, *11* (1), 2035.
- (44) Yin, J.; Maity, P.; Naphade, R.; Cheng, B.; He, J.-H.; Bakr, O. M.; Brédas, J.-L.; Mohammed, O. F. Tuning Hot Carrier Cooling Dynamics by Dielectric Confinement in Two-Dimensional Hybrid Perovskite Crystals. *ACS Nano* **2019**, *13* (11), 12621–12629.